Geophysical Journal International

Geophys. J. Int. (2015) **203,** 2119–2124 doi: 10.1093/gji/ggv412
GJI Seismology

The aftershock sequence of the 2015 April 25 Gorkha–Nepal earthquake

L.B. Adhikari,[1] U.P. Gautam,[1] B.P. Koirala,[1] M. Bhattarai,[1] T. Kandel,[2] R.M. Gupta,[1] C. Timsina,[1] N. Maharjan,[1] K. Maharjan,[2] T. Dahal,[2] R. Hoste-Colomer,[3,4] Y. Cano,[3] M. Dandine,[3] A. Guilhem,[3] S. Merrer,[3] P. Roudil[3] and L. Bollinger[3]

[1] *National Seismological Centre, Department of Mines and Geology, Lainchaur, Kathmandu, Nepal. E-mail: adhikari.research@gmail.com*
[2] *Regional Seismological Centre, Department of Mines and Geology, Surkhet-Birendranagar, Nepal*
[3] *CEA, DAM, DIF, F-*91297 *Arpajon, France*
[4] *Laboratoire de Géologie, Ecole Normale Supérieure, CNRS,* 24 *rue Lhomond, F-*75004 *Paris, France*

Accepted 2015 September 24. Received 2015 September 24; in original form 2015 July 13

SUMMARY

The *M* 7.8 2015 April 25 Gorkha earthquake devastated the mountainous southern rim of the High Himalayan range in central Nepal. The main shock was followed by 553 earthquakes of local magnitude greater than 4.0 within the first 45 days. In this study, we present and qualify the bulletin of the permanent National Seismological Centre network to determine the spatio-temporal distribution of the aftershocks. The Gorkha sequence defines a ∼140-km-long ESE trending structure, parallel to the mountain range, abutting on the presumed extension of the rupture plane of the 1934 *M* 8.4 earthquake. In addition, we observe a second seismicity belt located southward, under the Kathmandu basin and in the northern part of the Mahabarat range. Many aftershocks of the Gorkha earthquake sequence have been felt by the 3 millions inhabitants of the Kathmandu valley.

Key words: Earthquake source observations; Seismicity and tectonics; Asia.

1 INTRODUCTION

On 2015 April 25 at 11 h 56 local time, a M_w 7.8 (M_L 7.6) earthquake struck central Nepal devastating the region at the rim of the High Himalayan range and affecting Kathmandu valley, causing 8700+ deaths and leaving hundreds of thousands homeless. The regions affected by the main shock are located above the Main Himalayan Thrust fault (MHT), a shallow dipping megathrust accommodating half the India–Eurasia convergence where most of the shortening between India plate and the Tibetan plateau occurs (e.g. Bilham *et al.* 1997; Bettinelli *et al.* 2006).

While the northern deep portion of the thrust, under the high Himalayan range, continuously slips at 18 mm yr^{-1} during the interseismic period, its southern and shallowest segment is fully locked (e.g. Bollinger *et al.* 2004; Ader *et al.* 2012; Grandin *et al.* 2012). The locked portion of the fault system is estimated to extend over a distance of approximately 80 km from the surface trace of the Main Frontal Thrust that merges at depth on the MHT to the brittle–ductile transition, which falls at 15–20 km depth, under the southern slope of the high topography (Ader *et al.* 2012).

This segment partially ruptured during past large earthquakes. Such events include the $M \sim 7.5$ 1833 A.D. earthquake known by its macroseismic effects (Bilham 1995; Ambraseys & Douglas 2004; Szeliga *et al.* 2010), which suggest a partial rupture of the MHT, north of Kathmandu. In 1934, the larger Bihar–Nepal earthquake ($M \sim 8.2$–8.4) ruptured up to the surface along a minimum 150-km-long segment of the MHT, in eastern Nepal (Fig. 1; Sapkota *et al.* 2013).

Despite the significant documentation of these past events, their aftershock distribution is poorly known. This inhibits any detailed analysis of the seismic hazards following a large Himalayan earthquake, and prevents any discussion about the post-main shock slip potency. The recent Gorkha earthquake sequence helps toward better understanding the faulting conditions of the region. Here, we examine the aftershock sequence of the Gorkha earthquake recorded by the Nepal seismological network. We evaluate the quality of the early bulletins published by the National and Regional Seismological Centres. We then describe a homogeneous catalogue of aftershocks between 2015 April 25 and June 8, and we study their spatio-temporal distribution. We confront it to the available data from the 1833 and 1934 events. Such rapid earthquake catalogue is

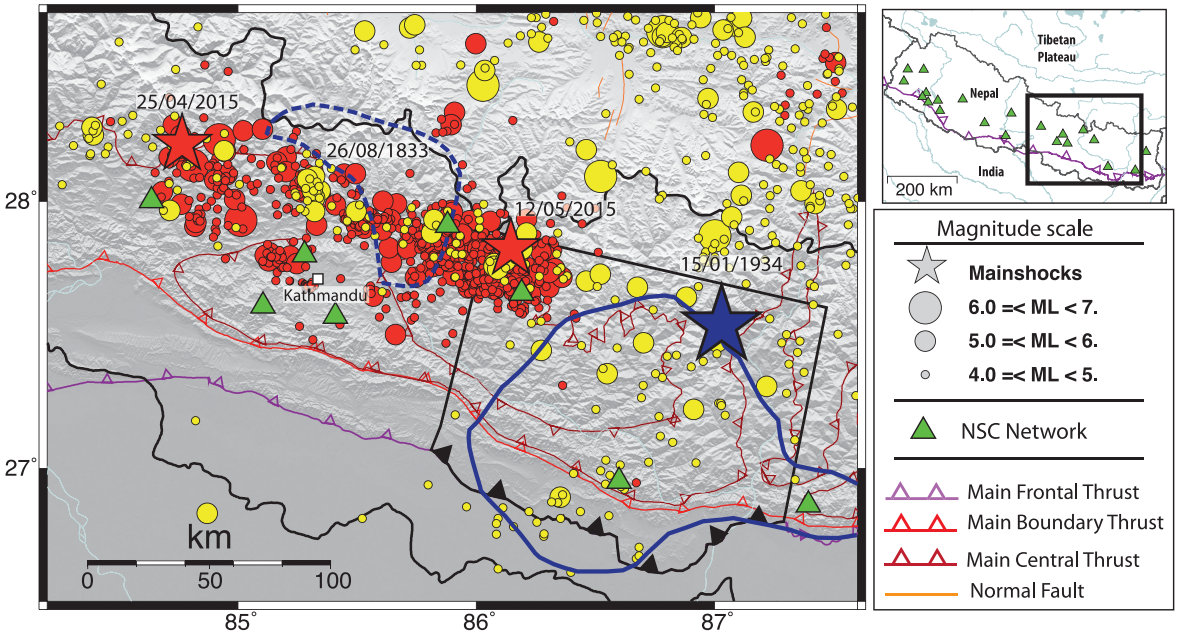

Figure 1. General map of the principal aftershocks (red dots) of the April 25th Gorkha earthquake located by NSC within the 45 days following the earthquake (red dots). Green triangles correspond to the national seismic network stations. The most western red star corresponds to the epicentre of the Gorkha earthquake while the eastern red star locates the epicentre of the May 12th event. In yellow, earthquake epicentres of the seismic events recorded during the twenty years preceding the main shock. Blue polylines correspond to the macroseismic isoseimals MSK64-VIII of the great 26/08/1833 and 15/01/1934 earthquakes (respectively dashed and plain polylines) deduced from Ambraseys and Douglas (2004) (Sapkota 2011). The blue star locates the relocated instrumental 1934 epicentre (Chen & Molnar 1977). Black rectangular polyline corresponds to the suspected extent of that earthquake rupture as suggested by (a) the macroseismic isoseismals and (b) the minimum stretch of 1934 MFT surface rupture represented by the black teethed polyline (Sapkota *et al.* 2013; Bollinger *et al.* 2014).

aimed to serve as a basic constraint to develop improved static and dynamic source models of the Gorkha earthquake, ultimately leading to a better understanding of strain and stress accommodation and release during the 2015 sequence.

2 METHODS AND BULLETIN ANALYSIS

2.1 Seismic data

In this study, we analyse seismic signals recorded by the Nepal nationwide seismological network (e.g. Pandey *et al.* 1995, 1999). 21 short period (1 s) vertical component stations (ZM500) and two broad-band (0.1–120 s) stations are operated by the Department of Mines and Geology (DMG) in collaboration with the Département Analyse Surveillance Environnement (DASE, France). These seismic stations are telemetered to, and processed at two independent seismic centres: the National Seismological Centre (NSC) and the Regional Seismological Centre (RSC). The NSC, which is located in Kathmandu, monitors the central and eastern Nepal seismicity with 12 analogous seismic stations deployed between 1978 and 1994. These records are digitized at the seismological centre. The RSC, based in Surkhet-Birendranagar, monitors the western Nepal seismicity with nine analogous stations deployed between 1994 and 1999 and later replaced in 2014 by digital stations. The records are all integrated, at both seismic centres, into the Jade-Onyx acquisition-treatment software suite. A three-layer 1-D velocity model is used for routine localisation processing. The *P*- and *S*-wave velocities in the three layers are, respectively (5.56, 6.50, 8.10) and (3.18, 3.71, 4.63) km s^{-1} with depth interfaces at 23 and 55 km for the Moho discontinuity (Pandey 1985; Pandey *et al.* 1995).

2.2 Magnitudes and locations

The local magnitude (M_L) is estimated on the maximum amplitude [$A(i)$] of the Sg, Sn or Lg seismic phases measured at station i on the 0.3–7 Hz bandpass filtered seismic signals following:

$$M_L\_\mathrm{NSC}(i) = \mathrm{LOG}[A(i)/T] + B[\mathbf{\Delta}(i)] + C(i), \quad (1)$$

where T is the period, B the attenuation law, and $C(i)$ a station correction term. The attenuation law is expressed as a function of the epicentral distance ($\mathbf{\Delta}$) and include a geometrical spreading correction and an anelastic attenuation term such that

$$B(\mathbf{\Delta}) = -1.85 + 0.854\ \log 10(\mathbf{\Delta}) + 0.00102\ \mathbf{\Delta}. \quad (2)$$

Only stations with epicentral distances greater than 100 km are considered for this magnitude determination, in order to avoid source and path effects. However, because the seismic signal saturates at most of the closest NSC stations during the largest earthquakes of the sequence, the measurement of the magnitude is limited to the stations located at the periphery of NSC network or to the stations of the RSC network.

Overall, 4401 events were manually picked and located within the 45 days following the main shock (between 2015 May 25 and June 8). 1802 events have M_L greater than 3.0 including 553 events with M_L greater than 4.0.

Regarding the events with M_L greater than 3.0, we estimate that their location is globally well constrained. Indeed, an average of 15–20 seismic phases was picked at NSC per event (Fig. 2). The minimal epicentral distance is lower than 31 km for 75 per cent of the events (Fig. 2a). Because of the geometry of the seismic cluster within the network, the maximal gap between two stations for a given event is preferentially 180–185° (Fig. 2b). However, origins of the easternmost epicentres (i.e. beyond longitude 86°)

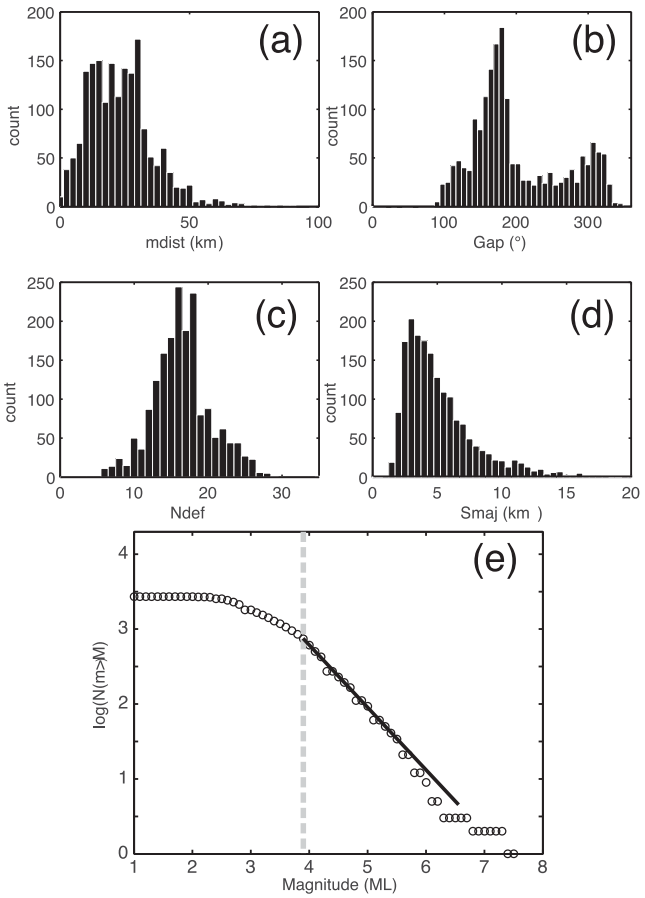

Figure 2. (a) Distance between the epicentre and the closest station. (b) Maximum azimuthal gap. (c) Number of phases pointed by events. (d) Major semi axis of the location uncertainty in kilometres. (e) Gutenberg–Richter plot of the cumulative number of events located by NSC analysts during the first 45 d after the Gorkha-earthquake main shock. The straight-line portion of the curve yields a *b*-value of 0.80 ± 0.05, while the progressive flattening of the curve below M_L 4 is the result of the incompleteness of the seismic catalogue below this value.

have an azimuthal gap around 300–310° between April 27 and May 28, due to a technical issue on a relay transmitting the easternmost stations (TAPN/ODAN/RAMN). Consequently, uncertainties on the locations of the earthquake cluster associated to the M 7.3 aftershock that followed on 2015 May 12 are larger than during the rest of the sequence. All those characteristics lead to a major semi axis of the location uncertainty ellipse with a median value at 4.7 km and a 95th percentile at 11.5 km (Fig. 2d). In total, analysts at DMG manually picked 55 778 phases, mainly Pg and Sg, through June 8 (Fig. 2c). The distribution of Pg and Sg time residuals show that the observed arrival times are consistent with the 1-D velocity model (Fig. S2). The average *Vp*/*Vs* ratio based on the entire catalogue is estimated at 1.70 ± 0.20 using *Ts*–*Tp* time difference. This value fits well with the theoretical *Vp*/*Vs* ratio used in the velocity model (i.e. $Vp/Vs = 1.75$).

RSC provided also bulletins of the sequence. These bulletins were merged to NSC's. However, because all the RSC stations recorded the events within a narrow azimuth/distance range of about [$280 \pm 20°$; 400 ± 100 km], their addition in the location process introduces a location bias that translates the epicentres by [−5; 30] km southward (Fig. S3). Longitudinal variations of the relocation vectors are smaller than latitudinal variations (i.e. in the [−5; +5] km range) and show no apparent regional trend. This potential bias could possibly be corrected after adding station corrections or by considering another velocity model. Such corrections are however outside of the scope of the present work. Here, we only exploit RSC bulletins regarding the magnitude associated to each event. Initial depths are obtained using the 1-D-layer model. As a result, the preliminary depth estimations clearly depict a layered structure consistent with the default depths of the location processing (originally set at 2/10/25/30/40/50 km and lately complemented for some events with additional values at 6/15 and 20 km). To obtain a clearer image of the aftershocks cluster at depth, we perform a relocation of the seismic sequence using ISClocator (Bondár & Storchak 2011) and taking into account the RSTT velocity model, a 3-D model including regional phase traveltime corrections (Myers *et al.* 2010). The relocation of the 4401 events studied, using ISClocator with RSTT and allowing for phase reallocation differs by 2.5 ± 4.2 km (median value) from the original NSC location. The main differences in term of earthquake locations between the two catalogues are illustrated on Figs S4–S6. The relocation confirms that most aftershocks are located in the hangingwall of the Main Himalayan Thrust.

2.3 Gutenberg–Richter distribution of the Gorkha sequence

Despite the 4401 events located by the seismic analysts, the seismic catalogue is clearly incomplete below $M_L = 4.0$ (Fig. 2e), which corresponds approximately to the magnitude of completeness (M_c). This magnitude is greater than the M_c determined during the interseismic period (i.e. $M_c \sim 2.0$) according to Pandey *et al.* (1999), even considering its season variations of ±0.5 magnitude unit due to the seismic noise of the rivers and landslides (Bollinger *et al.* 2007). The current M_c of the Gorkha sequence can be explained by (i) the high seismic noise level during the first hours following the main shock (Fig. S1), and (ii) the high number of seismic alerts during the early sequence. Indeed, NSC has for mission to provide rapid seismic alerts to the Nepalese authorities for all M_L 4.0+ earthquakes. Such requirements precluded picking arrivals for events smaller than M_L 4.0.

On the Gutenberg–Richter plot of the aftershocks (Fig. 2e), the straight portion of the cumulative number of seismic events as a function of the magnitude yields a *b*-value of 0.80 ± 0.05. This post-earthquake *b*-value is smaller than the average *b*-value of 1 observed worldwide, but identical within uncertainties to the average value of 0.83 ± 0.05 estimated between 1995 and 2015 in the same area from 2102 events of magnitude greater than 2.4, including 110 greater than M_L 4. We notice that there is a small overlap of the interseismic and post-seismic magnitude bands considered in the magnitude distributions that does not help for discussing in greater details the pre- and post-earthquake *b*-values.

3 SPATIO-TEMPORAL VARIATIONS OF THE SEISMICITY

The main shock was immediately followed by a string of aftershocks from its epicentre, near Barpak-Gorkha, to a region about 120 km to the east, within a trace width of about 40 km (Fig. 3). Altogether, more than 120 events with M_L greater than 4.0 were located there within the 12 hr following the main shock. The rate of the seismicity over the next 18 days showed a typical decay, and the aftershocks

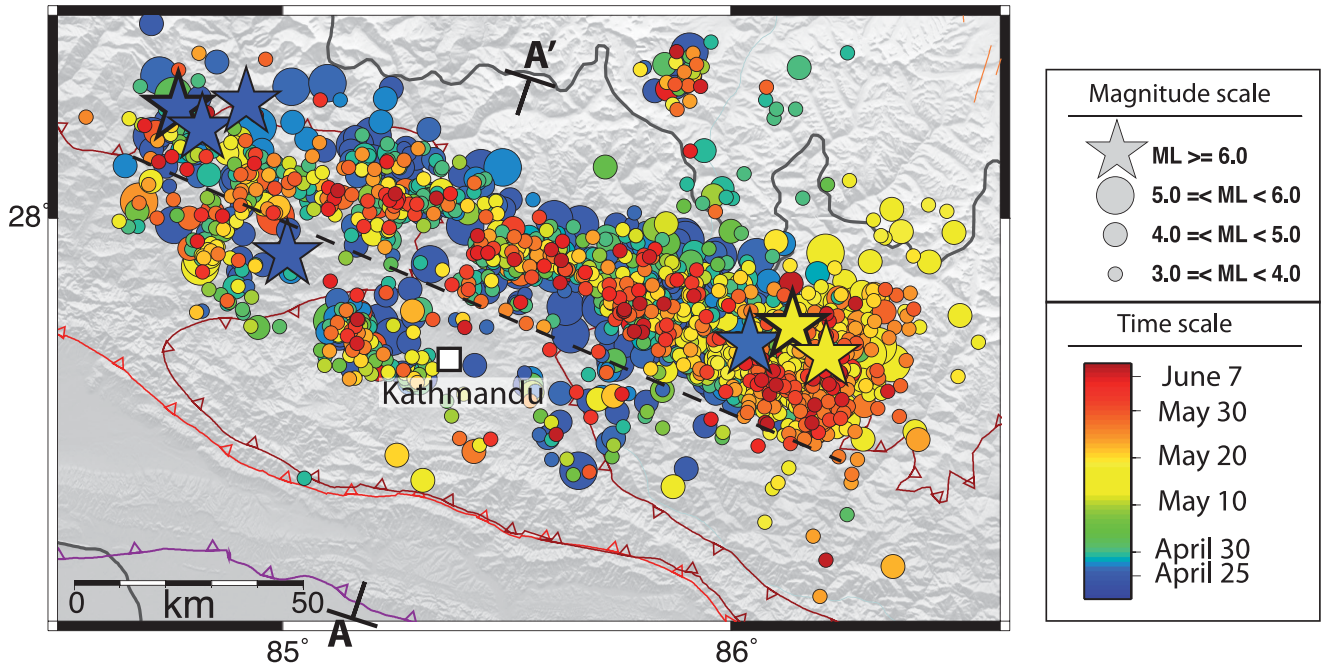

Figure 3. Map of the main shock and aftershocks of the Gorkha earthquake colour coded as a function of their time of occurrence. The dashed line divides the earthquake epicentres colour-coded in green (north) and red (south) on Fig. 4. Included on the map is the location of the A–A′ profile through the aftershocks (Figs S5a and b).

occurred within a relatively restricted area. The largest early aftershocks were located within the first 2 days at both the west and east termini of the main shock rupture (Fig. 3). Two large aftershocks with $M_L \geq 6.0$ immediately followed the main shock (i.e. 4 and 34 min, respectively) in its immediate vicinity at the western end of the cluster (Fig. 4). Its eastern end was also the place of two additional events of similar size ~3 and 25 hr, respectively after the main shock. The first of these events was located about 10 km east of its eastern rim, and was followed by a small cluster of events (Fig. 4).

Seventeen days later, on May 12, the largest aftershock (M_w 7.3, M_L 6.9) ruptured the easternmost region. This event was followed by an important number of aftershocks. We indeed counted almost 70 M_L 4+ events within the first 24 hr of the M 7.3 earthquake. These events were spread along a 60-km-long segment centred on the M 7.3 epicentre. In addition, a significantly denser cluster developed asymmetrically within a 30-km-large area, from about 10 km to the west to 20 km to the east of the epicentre (Fig. 4). The following large M_L 6.3 aftershock was recorded in this area about 30 min after. This seismic cluster remained very productive during the following weeks (Fig. 4).

The space–time distribution of all aftershocks within the first 45 days of the sequence reveals a clustering of activity within the main shock rupture zone (Fig. 4a). Because the clusters do not extend continuously from the downdip to the updip ends of the seismicity, we choose to separately divide the seismic area into two regions (see Fig. 3): a region to the south, comprising the trace of the Kathmandu basin and northern Mahabarat range, and another region to the north, covering the area devastated by the main shock (Figs 3 and 4). The temporal behaviour of seismicity in both areas (red for southern seismicity and green for the northern seismicity in Fig. 4) shows no significant differences. The clusters south of Kathmandu develop from the first day of the sequence, and depict a temporal decay similar to the one observed for the northern clusters (Fig. 4).

4 DISCUSSION – CONCLUSION

Most of the 3000 aftershocks located by NSC within the first 45 days following the Gorkha earthquake are concentrated in a narrow 40-km-wide band at midcrustal to shallow depths (i.e., between 2 and 25 km) along the strike of the southern slope of the high Himalayan range. The westernmost seismicity of the sequence near the M 7.8 epicentre seems to abut on a topographical high. Eastward, the seismicity develops within 160 km in two main clusters: (1) a large 120 × 40–50 km seismic patch, that activated immediately after the main shock and that encompassed significant spatial variations in term of seismicity rate, including a central area with a low rate of events and (2) a second smaller but denser patch (20 km × 30 km) located at the eastern end of the seismic cluster that mainly occurred following the May 12 earthquake (Figs 3 and 4). While the downdip end of the seismicity band along strike coincides broadly with the downdip end of the interseismic midcrustal cluster (Fig. 1), its updip extension develops significantly farther south. It is particularly true for the trace of the first, larger patch, where an embayment of the seismicity reaches the Chandragiri hills, ~50 km south from the onset of the seismicity. This first patch appears to coincide with the main fault segment and centred on the Kathmandu klippe. Teleseismic source inversions coupled with cGPS and DinSAR models show that the M 7.8 earthquake ruptured this segment (e.g. Avouac *et al.* 2015; Galetzka *et al.* 2015; Grandin *et al.* 2015), which may have also previously ruptured during the 1833 A.D. earthquake as suggested from the macroseismic trace of that 182-yr-old event (Martin *et al.* 2015 and Fig. 1). The second, smaller patch marks a deeper structural rupture further to the east that borders the north westernmost extent of the great 1934 AD earthquake (Fig. 1).

The characteristics of the main rupture that (1) is centred on the Kathmandu klippe, (2) probably occurred in a similar region as a past earthquake and (3) showed a two-step activation with along strike variations of the updip-end of the seismicity advocate for a potential midcrustal structure controlling the rupture extension

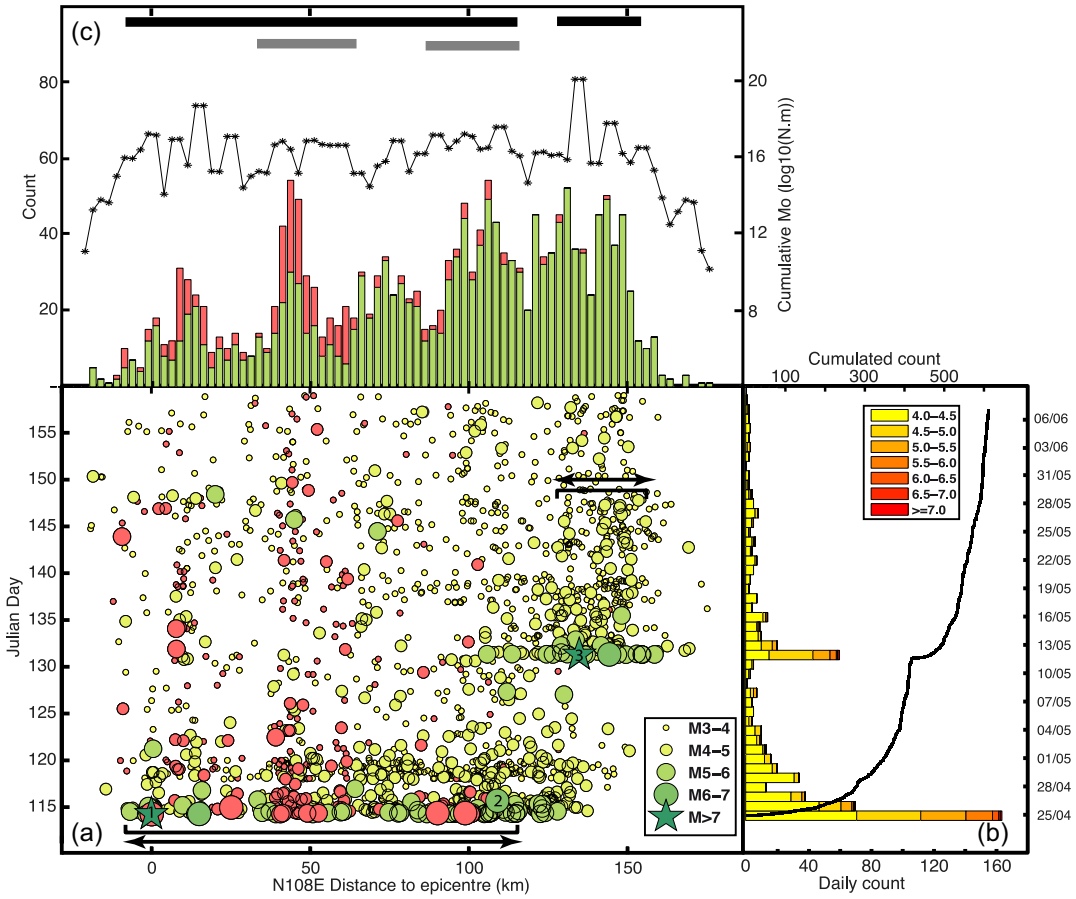

Figure 4. Spatio-temporal variation of the aftershocks. (a) Time sequence of the aftershocks. The events colour coded in red and green are respectively located south and north from the dashed line on Fig. 3. Numbers 1, 2 and 3 correspond, respectively, to the main shock epicentre, to the easternmost $M_L > 6.0$ event located within the supposed trace of the main shock and to the epicentre of the May 12th earthquake (underlined by the double arrows). (b) Daily and cumulated number of aftershocks with M_L greater than 4.0 (respectively histogram and black curve). (c) Lateral variations of the number of events (histogram) and moment released by the aftershocks.

of the earthquakes in this region of central Nepal. Moreover, the uneven along-strike distribution of aftershocks may reflect second-order structural features and/or lateral variations of co- and post-seismic slip (e.g. Avouac *et al.* 2015; Grandin *et al.* 2015). Both need to be better understood given their potential control on future rupture extensions.

After 45 days of aftershock activity, the rate of events with magnitudes above the present completeness magnitude (i.e. $M_c \sim 4$) has remained high (>1 per day) compared to the rate of five events of similar size recorded per year in the last 20 yr for the area covered by the post-seismic activity (Fig. 1). This present-day rate is, however, consistent with a typical temporal decay of the number of events. Analysis of the catalogue shows that the $M4+$ aftershock rate, $R(t)$, as a function of time, t, since the main shock follows a modified Omori law such as:

$$R(t) = k(t + c)^{-p}, \tag{3}$$

where $p = 0.8 \pm 0.4$, $c = 0.019 \pm 0.015$ and $k = 30.92 \pm 2.97$ for the main cluster, and $p = 0.78 \pm 0.07$, $c = 0.004 \pm 0.012$ and $k = 11.21 \pm 1.44$ within the trace of M 7.3 May 12 aftershock. We find that k, which is normalized to the surface considered, appears larger within the trace of that aftershock. We also stress that c is probably ill-defined due to the fact that some M_L 4+ aftershocks were almost certainly missed during the day following the main shock given the high level of background seismic noise (Fig. S1) and the saturation of the seismic stations. p is similar within the uncertainty for the two patches and well within the range of p values 0.6–2.5 previously reported (Utsu & Ogata 1995), smaller than the value of 1.15 obtained for Muzzafarabad-2005 (Tahir & Grasso 2013). These values of the p parameter are within typical average values for thrust faults [i.e. around 0.8 according to Tahir (2011)].

However, because both MHT fault segments located (i) south to the Gorkha rupture and (ii) west of it are capable of generating large earthquakes, monitoring the behaviour of the seismicity around the Kathmandu valley will remain crucial. In the meantime, additional work on the aftershock activity, preferentially focusing on the generation of a catalogue of smaller sized earthquakes and on their precise relocations, will be important to assess and understand eventual migration of seismicity on the MHT and on surrounding splay faults that may add to the regional seismic hazards.

ACKNOWLEDGEMENTS

The authors are most grateful to Mr Sarbajit Prasad Mahato, director of DMG and Soma Nath Sapkota, Deputy Director General in charge of the Geoscience division as well as to all the staff of the DMG and DASE who have contributed to the national seismological network. Eric Sauvage and JeanBaptiste Leblanc, which collaborated in maintaining the network during the seismic crisis

are also thanked. We also thank Susan Hough and Pascal Bernard for their constructive reviews as well as Helene Lyon-Caen, Jean Letort and Christian Baillard for useful discussions.

REFERENCES

Ader, T. *et al.*, 2012. Convergence rate across the Nepal Himalaya and interseismic coupling on the Main Himalayan Thrust: implications for seismic hazard, *J. geophys. Res.,* **117,** B04403, doi:10.1029/2011JB009071.

Ambraseys, N.N. & Douglas, J., 2004. Magnitude calibration of north Indian earthquakes, *Geophys. J. Int.,* **159,** 165–206.

Avouac, J.P., Meng, L., Wei, S., Wang, T. & Ampuero, J.P., 2015. Lower edge of locked Main Himalayan Thrust unzipped by the 2015 Gorkha earthquake, *Nat. Geosci.,* **8,** 708–711.

Bettinelli, P., Avouac, J.P., Flouzat, M., Jouanne, F., Bollinger, L., Willis, P. & Chitrakar, G.R., 2006. Plate motion of India and interseismic strain in the Nepal Himalaya from GPS and DORIS measurements, *J. Geod.,* **80**(8–11), 567–589.

Bilham, R., 1995. Location and magnitude of the 1833 Nepal earthquake and its relation to the rupture zones of contiguous great Himalayan earthquakes, *Curr. Sci.,* **69,** 101–128.

Bilham, R. *et al.*, 1997. GPS measurements of present-day convergence across the Nepal Himalaya, *Nature,* **386**(6620), 61–64.

Bollinger, L., Avouac, J.P., Cattin, R. & Pandey, M.R., 2004. Stress build up in the Himalaya, *J. geophys. Res.,* **109,** B11405, doi:10.1029/2003JB002911.

Bollinger, L., Perrier, F., Avouac, J.P., Sapkota, S., Gautam, U. & Tiwari, D.R., 2007. Seasonal modulation of seismicity in the Himalaya of Nepal, *Geophys. Res. Lett.,* **34,** L08304, doi:10.1029/2006GL029192.

Bollinger, L. *et al.*, 2014. Estimating the return times of great Himalayan earthquakes in Eastern Nepal: evidence from the Patu and Bardibas strands of the Main Frontal Thrust, *J. geophys. Res.,* **119**(9), 7123–7163.

Bondár, I. & Storchak, D., 2011. Improved location procedures at the International Seismological Centre, *Geophys. J. Int.,* **186**(3), 1220–1244.

Chen, W.-P. & Molnar, P., 1977. Seismic moments of major earthquakes and the average rate of slip in Central Asia, *J. geophys. Res.,* **82,** 2945–2969.

Galetzka, J. *et al.*, 2015. Slip pulse and resonance of Kathmandu basin during the 2015 M_w 7.8 Gorkha earthquake, Nepal imaged with geodesy, *Science,* **349,** 1091–1095.

Grandin, R., Doin, M.P., Bollinger, L., Pinel-Puyssegur, B., Ducret, G., Jolivet, R. & Sapkota, S.N., 2012. Long-term growth of the Himalaya inferred from interseismic InSAR measurement, *Geology,* **40**(12), 1059–1062.

Grandin, R., Vallée, M., Satriano, C., Lacassin, R., Klinger, Y., Simoes, M. & Bollinger, L., 2015. Rupture process of the M_w = 7.9 2015 Gorkha earthquake (Nepal): insights into Himalayan megathrust segmentation, *Geophys. Res. Lett.,* doi:10.1002/2015GL066044.

Martin, S., Hough, S., Bilham, R. & Hung, C., 2015. Ground Motions from the 2015 M7.8 1 Gorkha, Nepal, Earthquake Constrained by a Detailed Assessment of Macroseismic Data, Accepted at Seismological Research Letters, special issue on Gorkha earthquake.

Myers, S.C. *et al.*, 2010. A crust and upper mantle model of Eurasia and North Africa for Pn travel-time calculations, *Bull. seism. Soc. Am.,* **100,** 640–656.

Pandey, M.R., 1985. Seismic model of central and eastern lesser Himalaya of Nepal, *J. Nepal geol. Soc.,* **3**(1–2), 1–11.

Pandey, M.R., Tandukar, R.P., Avouac, J.P., Lavé, J. & Massot, J.P., 1995. Interseismic strain accumulation on the Himalayan Crustal Ramp (Nepal), *Geophys. Res. Lett.,* **22,** 751–754.

Pandey, M.R., Tandukar, R.P., Avouac, J.P., Vergne, J. & Héritier, T., 1999. Seismotectonics of the Nepal Himalayas from a local seismic network, *J. Asian Earth Sci.*, **17**(5–6), 703–712.

Sapkota, S.N., 2011. Surface rupture of 1934 Bihar-Nepal earthquake: implications for Seismic Hazard in Nepal Himalaya, *Unpublished thesis,* IPGP, pp. 1–292.

Sapkota, S.N., Bollinger, L., Klinger, Y., Tapponnier, P., Gaudemer, Y. & Tiwari, D., 2013. Primary surface rupture of the great Himalayan earthquakes of 1934 and 1255, *Nat. Geosci.,* **6,** 71–76.

Szeliga, W., Hough, S., Martin, S. & Bilham, R., 2010. Intensity, magnitude, location, and attenuation in India for felt earthquakes since 1762, *Bull. seism. Soc. Am.,* **100**(2), 570–584.

Tahir, M., 2011. Aftershock properties and its triggering mechanism, *PhD thesis,* Grenoble University, France.

Tahir, M. & Grasso, J.R., 2013. Aftershock patterns of $M_s > 7$ earthquakes in the India–Asia collision belt: anomalous results from the Muzaffarabad Earthquake sequence, Kashmir, 2005, *Bull. seism. Soc. Am.*, **104**(1), 1–23.

Utsu, T. & Ogata, Y., 1995. The centenary of the Omori formula for a decay law of aftershock activity, *J. Phys. Earth,* **43**(1), 1–33.

SUPPORTING INFORMATION

Additional Supporting Information may be found in the online version of this paper:

Figure S1. Time–frequency diagram of the power spectral density (in acceleration) at GKN. SHZ raw signals between day 100 and 150.

Figure S2. (a, b) Respectively histograms of the Pg and Sg residues in seconds (c) *Vp*/*Vs* estimation from t_S–t_P time difference.

Figure S3. Illustration of RSC/NSC bulletin fusions on the location of the epicentres (a) Map of the relocation vectors generated after the RSC/NSC bulletin fusion (b) Histograms of the latitudinal and longitudinal components of the relocation vectors.

Figure S4. Map view of hypocentre locations. (a) Using the default parameters (b) After relocation using ISClocator (Bondár & Storchak 2011) and taking into account the RSTT velocity model, a 3-D model including regional phase traveltime corrections (Myers *et al.* 2010). A–A′ locate the cross-section through the aftershocks Fig. S5. Note the deeper aftershocks along the trace of the eastern segment, ruptured on 2015 May 12.

Figure S5. Cross-sections through the aftershocks along A–A′ profiles (see location on Figs 3 and S4). All hypocentres within 20 km from the N18E profile going through Kathmandu are represented.

Figure S6. Hypocentres depth histograms (a) for the original bulletin and (b) After relocation using ISClocator (Bondár & Storchak 2011) and taking into account the RSTT velocity model, a 3-D model including regional phase traveltime corrections (Myers *et al.* 2010).

Table S1. Original NSC seismic catalogue of all aftershocks greater than M_L 4.0 for the 45 days following the Gorkha-Nepal earthquake.

Table S2. Seismic catalogue of all aftershocks greater than M_L 4.0 for the 45 days following the Gorkha-Nepal earthquake relocated using ISClocator taking into account RSTT velocity model—see paper for further details and references.

Table S3. GSE2 bulletin for the 45 days following the Gorkha-Nepal earthquake. This bulletin incorporates the Phasepicks/arrivals at each NSC station for all events with $M_L \geq 4.5$ (http://gji.oxfordjournals.org/lookup/suppl/doi:10.1093/gji/ggv412/-/DC1).

Please note: Oxford University Press is not responsible for the content or functionality of any supporting materials supplied by the authors. Any queries (other than missing material) should be directed to the corresponding author for the paper.